PAPER • **OPEN ACCESS**

Measurements regarding a combined therapy concept for ophthalmic tumors consisting of brachytherapy and x-rays

Biomedical Physics & Engineering Express

PAPER

Measurements regarding a combined therapy concept for ophthalmic tumors consisting of brachytherapy and x-rays

H Manke[1], D Fluehs[2], M Stroth[1], N E Bechrakis[2], A M H Foerster[2] and J Albrecht[1]

[1] Department of Physics, TU Dortmund University, Otto-Hahn-Str. 4a, 44227 Dortmund, Germany
[2] Radiation and Tumor Clinic, Essen University Hospital, Hufelandstr. 55, 45147 Essen, Germany

E-mail: henning.manke@tu-dortmund.de

Keywords: brachytherapy, ruthenium-106, x-rays, ophthalmic tumors, choroidal and uveal melanoma

OPEN ACCESS

RECEIVED
11 September 2023

REVISED
27 March 2024

ACCEPTED FOR PUBLICATION
8 April 2024

PUBLISHED
26 June 2024

Abstract

Objective. We present a novel concept to treat ophthalmic tumors which combines brachytherapy and low-energy x-ray therapy. Brachytherapy with ^{106}Ru applicators is inadequate for intraocular tumors with a height of 7 mm or more. This results from a steep dose gradient, and it is unfeasible to deliver the required dose at the tumor apex without exceeding the maximum tolerable sclera dose of usually 1000 Gy to 1500 Gy. Other modalities, such as irradiation with charged particles, may be individually contraindicated. A dose boost at the apex provided by a superficial x-ray therapy unit, performed simultaneously with the brachytherapy, results in a more homogeneous dose profile than brachytherapy alone. This avoids damage to organs at risk. The applicator may also serve as a beam stop for x-rays passing through the target volume, which reduces healthy tissue dosage. This study aims to investigate the suitability of the applicator to serve as a beam stop for the x-rays. *Approach.* A phantom with three detector types comprising a soft x-ray ionization chamber, radiochromic films, and a self-made scintillation detector was constructed to perform dosimetry. Measurements were performed using a conventional x-ray unit for superficial therapy to investigate the uncertainties of the phantom and the ability of the applicator to absorb x-rays. The manufacturer provided a dummy plaque to obtain x-ray dose profiles without noise from ^{106}Ru decays. *Results.* The phantom is generally feasible to obtain dose profiles with three different detector types. The interaction of x-rays with the silver of the applicator leads to an increased dose rate in front of the applicator. The dose rate of the x-rays is reduced by up to 90% behind a ^{106}Ru applicator. Therefore, a ^{106}Ru applicator can be used as a beam stop in combined x-ray and brachytherapy treatment.

1. Introduction

Untreated intraocular tumors pose a life-threatening risk. Experienced clinics report tumor control rate for uveal and choroidal melanoma of more than 90% (Flühs *et al* 2004). As no general therapy concept for intraocular tumors exists and a single clinic may not be able to provide all treatment options, clinics vary in indications and contraindications for the different treatments. Since the 1960s, the standard modality in Europe has been brachytherapy with ^{106}Ru applicators (Lommatzsch and Vollmar 1966). The used applicators, also called plaques, comprise a silver calotte with a thin radioactive layer inside (Bornfeld *et al* 2004, BEBIG 2013). The decay chain of ^{106}Ru includes ^{106}Rh, which emits electrons with a maximum energy of $E^{e-}_{max} = 3.54$ MeV (Bé *et al* 2016). ^{125}I is another isotope used for ocular brachytherapy, which is most often handled in the form of the so-called COMS-applicators consisting of a gold carrier with a silicone insert for iodine seeds. This isotope emits photons with a maximum energy of ≈32 keV (The Collaborative Ocular Melanoma Study Group 2001, Bé *et al* 2016). Both therapies have a limitation concerning the tumor height with a maximum of 7 mm for ^{106}Ru (Stöckel *et al* 2017, Tagliaferri *et al* 2020) and 9 mm for ^{125}I applicators (Flühs *et al* 2004). However, these limitations may be disregarded when the patient expressively requests that brachytherapy be attempted as an alternative to immediate enucleation of the eye in cases without other available treatment options. Since the summer of 2021, the bi-nuclide applicators

presented by Flühs *et al* (2004) and Ebenau (2017) have not been used at the University Hospital Essen anymore because the corresponding medical device approval has expired.

Proton therapy, a fast-growing radiotherapeutic option, has also been used for about 40 years. However, proton therapy for ophthalmic tumors is only accessible at approximately 20 centers worldwide (Fleury *et al* 2021). Most clinics deliver the dose for ophthalmic tumors with a single field per fraction. This leads to a relatively high dosage in tissue traversed by the proton before reaching the tumor (Desjardins *et al* 2011, Tarlan and Kıratlı, 2016, Foti *et al* 2021). Tumors close to the optic nerve are sometimes treated with a safety margin that includes parts of the optic nerve (Paganetti 2012, Seibel *et al* 2015). Compared to plaque therapy, the rates of enucleation, vision loss, and neovascular glaucoma are potentially higher after proton beam therapy (Tseng *et al* 2016). This is possibly an effect of different indication criteria for brachytherapy and proton therapy. A comparative study for brachytherapy and proton therapy, including tumors with comparable clinical parameters, could not be found. Surgical resection may be used before or after a radiotherapeutic treatment to prevent toxic tumor syndrome associated with higher tumor volumes (Böker *et al* 2018, Rauchegger *et al* 2020, Damato *et al* 2013), or to decrease tumor volume in general for any radiotherapeutic option.

Stereotactic radiosurgery is also used in some clinics, as reported by, e.g., Eibl-Lindner *et al* (2016), Mor *et al* (2017), Sekac *et al* (2019), Mazzini *et al* (2020) and Schmelter *et al* (2022b, 2022a). The available literature lacked extensive studies with large patient cohorts. In Eibl-Lindner *et al* (2016), the presented 5-year tumor control rate of 70.3% is significantly lower than for other modalities. This may be due to the rather low mean prescribed dose of 20.3 Gy at the 69% isodose. A tumor recurrence rate of 12.4% is stated by Schmelter *et al* (2022b).

An internal statistic of the University Hospital Essen shows that 10.4% of the diagnosed tumors have a height of >7 mm. These tumors cannot be treated with any model of the ^{106}Ru applicators due to the steep dose gradient. Furthermore, 9.4% of the tumors have a height of 6 mm to 7 mm and may be treated with ^{106}Ru, but only with larger types such as CCB or CGD, often with an irradiated area much larger than the tumor base. In 2022, 328 brachytherapy treatments were performed at the University Hospital Essen, and 78 patients were treated with proton therapy. 132 enucleations were conducted, of which 112 were due to contraindications for the bulb-preserving modalities.

We want to investigate a new therapy concept for intraocular and especially highly prominent tumors, as enucleation greatly impacts quality of life, and bulb-preserving modalities may be individually contraindicated. We developed a therapy concept combining brachytherapy and low-energy x-rays provided by a refined superficial x-ray therapy unit. The quality of brachytherapy for ophthalmic tumors might be improved by the dose boost provided with x-rays.

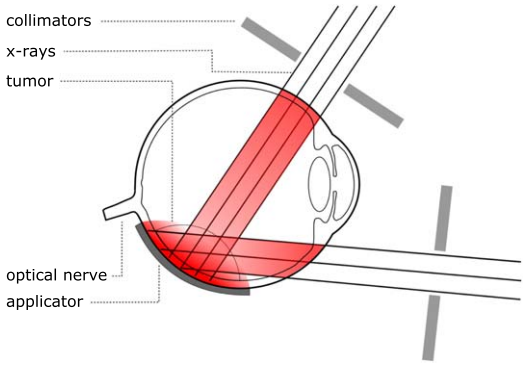

Figure 1. Illustration of a generic eye with a tumor treated with the combined therapy concept comprising x-rays and the ^{106}Ru applicator. For visual reasons, only two collimated x-ray beams are depicted in this example. The x-rays enter the eye through or near the radiation-insensitive pars plana. With confocal irradiation, a dose boost is applied to the tumor, particularly the region furthest from the applicator. The photons are absorbed in the silver plaque. The potential dose profiles of the different modalities are illustrated in red. The sizes and the dose profiles are not to scale.

1.1. The combined therapy concept

Our novel concept, visualized in figure 1, was first presented by H Manke (2023) and consists of ^{106}Ru brachytherapy and low-energy x-rays. While the dose profile of the plaque decreases rapidly toward the tumor apex, the x-rays provide a dose boost in these tumor regions. Once the advantages of the confocal irradiation technique are considered with beam entry areas at different points through the pars plana, healthy tissue can be significantly spared. Furthermore, the x-ray therapy might take place during the application time of the ^{106}Ru plaque. The plaque represents a 1 mm thick target made of silver, which can absorb most of the x-rays that have already passed the tumor. This way, healthy tissue located behind the eye is spared regarding the x-rays.

The application time of the ^{106}Ru applicator in combination with x-rays is shorter than for standalone brachytherapy due to the additional delivered dose. Using the applicator as a beam-stop for the x-rays, leads to a timing window of approximately 1 d to 5 d for the x-ray therapy. Also, it could be considered to perform the x-ray therapy right after the plaque application, as the patient is still under anesthesia.

In this study, we want to measure the suitability of the ^{106}Ru to serve as a beam stop for low-energy x-rays. To obtain and evaluate the dosimetric basis of the combined therapy concept, we constructed a solid phantom in which three different detector types can be used: self-made scintillation detectors, a soft x-ray chamber, and radiochromic films.

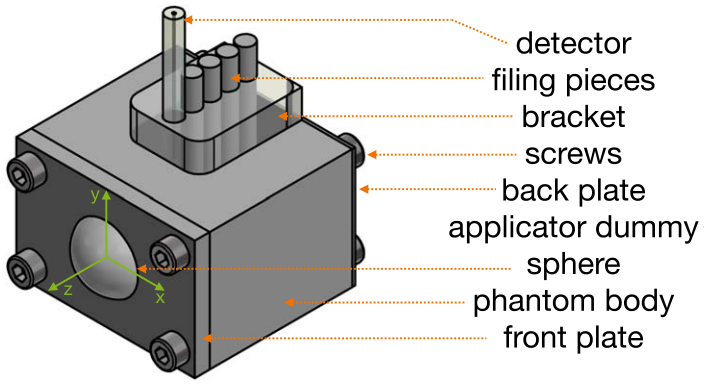

Figure 2. Illustration of the PWLR phantom with a scintillation detector included. On the left, a view from a top right front angle is shown. Furthermore, the used coordinate system is pictured. The graphic on the right shows a sectional view from the top.

2. Theoretical and experimental methods

The experiment used to acquire dose profiles of x-rays with or without interference with a non-radiating dummy applicator consists of a superficial x-ray therapy unit, a solid phantom, and three detector types.

2.1. The superficial x-ray therapy unit

The measurements were performed with a T-105 x-ray therapy system distributed by BEBIG Medical GmbH, Berlin, Germany (BEBIG Medical—BEBIG Medical GmbH 2023). This therapy unit is mainly used to treat target volumes at surfaces or shallow depths in the range of mm to few cm. It has a maximum acceleration voltage of $U_{\mathrm{max}} = 100$ kV and a maximum output current of $I_{\mathrm{max}} = 12$ mA. For the measurements, two standard therapy profiles were chosen. The first consisted of $U_1 = 70$ kV acceleration voltage at $I_1 = 10$ mA filtered by 1 mm aluminium in addition to the inherent filter of 1 mm beryllium. The second radiation profile had an output current of $I_2 = 12$ mA at $U_2 = 100$ kV filtered by 0.5 mm copper externally. For the scintillation detectors described in section 2.3.3 an output current of $I_1^{\mathrm{S}} = 3$ mA with an acceleration voltage of $U_1 = 70$ kV was chosen. The round applicator of the superficial x-ray therapy unit used for measurements had a diameter of 15 mm (WOMed—Wolf-Medizintechnik GmbH 2023).

2.2. The phantom

The phantom design allowed for the measurements of photon depth dose curves interrupted by a ^{106}Ru applicator. To evaluate different detector types, the phantom could mount a soft x-ray ionization chamber type 34013 (see PTW—PTW Freiburg GmbH, 2016), radiochromic EBT-3 film (see Ashland—Ashland Inc., 2023a, 2023b) and self-made scintillation detectors. All detectors are further described in section 2.3.

To ensure a tissue equivalent measurement, the material Plastic Water® Low Range (PWLR) (CIRS—Computerized Imaging Reference Systems Inc 2023) was used for all parts of the phantom. The phantom consisted of a body where the plaque, a sphere, and a mounting device for detectors can be positioned (figure 2). The sphere represented the eye and has a diameter of 24 mm. The dummy applicator was positioned behind the sphere in a recess in the phantom body. The sphere and the brackets were kept in position by plates secured with four screws each. The front plate had a thickness of 10 mm while the backplate was only 1 mm thick. The three different setups for the various detector types are illustrated in figure 3. The mounting devices for the scintillation detector could be rotated by 180° and had four rounded edges. In comparison, the mounting devices for the soft x-ray chamber and the radiochromic film only had two rounded edges. The resulting gaps for the scintillation detector mounting devices were filled with precisely fitting PWLR pieces. The phantom was irradiated from the front or the back, with particles entering through the sphere or back plate. In the following, the flight direction of the particles is equated with the z-axis (see figure 2). The mounting devices ensured that the effective measuring point of the soft x-ray chamber and the scintillation detector were positioned on the z-axis. The radiochromic film's active area was placed in the x-z plane.

The mounting device for the soft x-ray chamber (see section 2.3.1) had a continuous opening along the irradiation axis into which the soft x-ray chamber could be inserted. The unfilled space is supplemented with PWLR pieces. With the geometry of the chamber, this lead to measuring points in the interval 0.06 mm to 27.06 mm within the bracket of the detector with a step size of 1 mm.

The radiochromic film (see section 2.3.2) allowed a two-dimensional dose measurement. To maximize the measured area, the whole area of the recess for the bracket was used. Therefore, the mounting device consists of a lower and an upper part. Furthermore, the film is the only detector type that could be used in front of the plaque. Two hemispheres with the film in between were positioned into the phantom for this

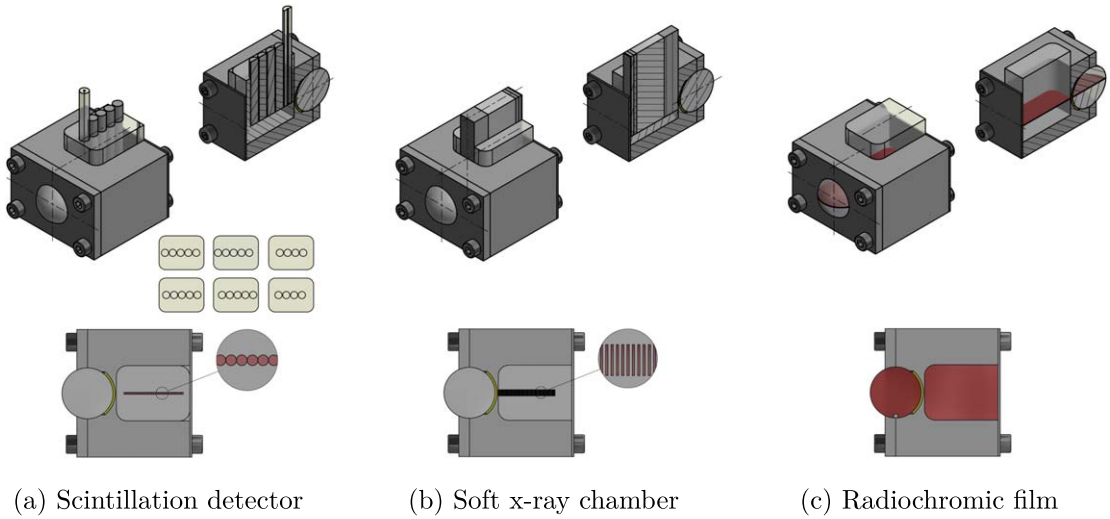

Figure 3. Illustration of the detector-specific setups of the PWLR phantom. The red areas represent the sensitive volumes of each detector type. For illustration purposes, in (a) the scintillation detectors are shown with a step size of 1 mm so that the sensitive volumes do not overlap. In (b), the setup is shown for the soft x-ray chamber while irradiated from the front. When the phantom is irradiated from the back, the chamber is turned, and therefore, the sensitive volumes are close to the back plate of the phantom. In (c), the radiochromic film setup is visualized.

purpose and aligned with the help of visual markings. One of the two hemispheres had a recess of 1 mm size on one side, while the other had the matching elevation. The films between those hemispheres had a matching cutout on one side. This cutout was always placed in the same position in the phantom, and therefore, it could be used to find the correct orientation in the scan of a round film. This is further described in section 2.3.2.

For the scintillation detector, six different mounting devices differing in the number and positioning of the holes for the detector were manufactured (see section 2.3.3). By combining the brackets in both possible orientations, a total of 56 measuring points with varying distances were achieved. The effective measuring points within the brackets were in the interval of 3.5 mm to 31.0 mm with a step size of 0.5 mm.

For measurements without ^{106}Ru radiation, a dummy applicator of type CCB was provided by the manufacturer Eckert & Ziegler BEBIG GmbH, Berlin, Germany. The dummy was manufactured in a standard plaque manner, excluding the deposition of radioactive material on the target foil. The silver plaque is 1 mm thick and had a diameter of 20.2 mm. The inner spherical radius was 12 mm (Eckert & Ziegler BEBIG GmbH 2022). More information on the plaques can be found in Eckert & Ziegler BEBIG GmbH (2022), Damato (2023) and Sommer *et al* (2017).

2.3. Detector types

2.3.1. Soft x-ray chamber

The soft x-ray ionization chamber (type 34013) is a thin window plane parallel chamber intended for photons of spectra in the range of 15 kV to 70 kV. At our request, the detector was further calibrated for a 100 kV spectrum by the manufacturer. With a sensitive volume of 0.005 cm^3, the chamber is mostly used for small-field dosimetry (PTW—PTW Freiburg GmbH, 2016). In our experiment, the readout was performed with a UNIDOS® Romeo in trigger mode (see PTW, 2020, 2021, and 2023 for further information). Dose rates $\dot{D}$ stated in section 3 were calculated by the measured integrated dose over beam time. The general uncertainty of measured values is stated to be 0.5%, and the calibration values are given with a relative uncertainty of 2% (PTW—PTW Freiburg GmbH 2016, PTW 2020, 2022b).

2.3.2. Radiochromic film

For the film measurements, EBT-3 dosimetry film produced by GAFChromic was used. The films consist of a 28 μm thick active layer between two matte surface transparent polyester base layers with a thickness of 125 μm. The films were cut according to the geometry of our phantom with an LS900 industrial laser engraver by Gravotech (see Gravotech GmbH, 2022). Film measurements were performed according to the guide for efficient and accurate film calibration and dosimetry provided by the manufacturer, which leads to a general uncertainty of 2% (Ashland—Ashland Inc., 2023a, 2023b).

Dose profiles were calculated using the FilmQA Pro test version with two different calibrations for both the 70 kV and the 100 kV spectrum measurements. The exported files were then further analyzed with a self-written Python script, first applying the manufacturer's specified uncertainty of 2% to each dose value. Furthermore, this script searched for the area with doses >0 and rotates the array so that all films can be directly compared. Two circles were found in the dose profile with the CV2 Hough Circles function (Open CV—Open Source Vision

Foundation, 2022) to calculate the rotation angle for round films. The first circle describes the small cutout, while the second is the general form of the films. For the larger films, the CV2 minAreaRect function (Open CV, 2023) was used. As the laser impaired the edge of the films, the first 20 pixels on each edge of each scan are ignored. Dose rates $\dot{D}$ were calculated by the measured dose over beam time and dose rates $\dot{D}$ of the same setup were averaged. The mean of the center 20 rows of the depth dose profile were calculated to obtain the depth dose curves, further reducing the uncertainty of these values. However, we think the uncertainty provided by the manufacturer is an underestimation regarding the data we collected, as further explained in the discussion.

2.3.3. Scintillation detectors

Our self-made scintillation detectors were built according to Eichmann (2017) with small changes due to measured radiation quality. As we did not expect Čerenkov light for these low-energy x-rays and their secondary particles, the detector had no AirCore implemented. Instead, the scintillator composed of polyethylene naphthalate was affixed directly to the light guide (specifically, type CWKF-1001 E22 manufactured by CUNZ GmbH & CO.KG, Darmstadt, Germany) with a protective light guide sheath encasing it. The scintillator had a thickness of 0.5 mm and a diameter of 1 mm. On the opposite side of the scintillator, a high-reflective foil (type PCM0080, produced by Hahn Polyfilms GmbH, Soltau, Germany) with a thickness of 8 μm was employed to enhance the signal. These components were then glued into a PWLR sleeve. To decrease noise by background light, the detector was painted black. The light produced by the scintillator was transmitted via the light guide to a photomultiplier tube (type H10721-210, Hamamatsu Photonics Deutschland GmbH, Herrsching, Germany) (Hamamatsu Photonics 2016, 2023). The scintillation detector was not calibrated. Therefore, the measured current I was not transferred into dose rates. All measured values were corrected for dark current signals, which were measured for the detector without radiation. The effective measuring point of the scintillator was assumed to be at its center (Eichmann 2010). The readout software averaged the current until the relative standard error descended below a threshold of 0.5%. Independent from this threshold, a minimum of 100 values were always considered, and the measurement was stopped after 30 s. For the scintillation detector, we assumed a systematic uncertainty of 2% based on (Eichmann 2010).

2.4. Measurements

The measurements described in this section were used to evaluate the suitability of the plaque to absorb the x-rays and to evaluate the uncertainties regarding the experiment. A more detailed description can be found in Manke (2023). The phantom was placed onto a fixed plate with a perpendicular recess to minimize position uncertainties. This allowed us to find the relative position between the phantom and the x-ray tube precisely after switching detector positions or the used detector itself. The measurements to analyze uncertainties of the phantom are described in section 2.4.1, while the experiment to investigate the suitability of the ^{106}Ru applicator as beam stop is presented in section 2.4.2.

2.4.1. Uncertainties

The uncertainties of the measured dose rate $\dot{D}$ and current I respectively were evaluated as specified in the following. Mostly, only one of the two spectra was used. The uncertainties were assumed to be very similar for the other spectrum. In the following, $\sigma_{\dot{D}}$ and σ_I are defined as the standard deviation of a set of $\dot{D}$ or I, respectively, while $\mu_{\dot{D}}$ and μ_I are the mean values of the corresponding set.

Position uncertainty With the soft x-ray chamber, the PWLR phantom was investigated by repositioning the phantom and the superficial x-ray therapy unit . In a depth of 21 mm the dose rate $\dot{D}$ was measured five times while irradiated with 100 kV photons. The relative uncertainty was considered as $\sigma_\mathrm{p} = \frac{\sigma_{\dot{D}}}{\mu_{\dot{D}}}$.

Current up and down scaling To calculate the uncertainty based on the current change, $n = 4$ points of a depth dose curve were measured three times with the soft x-ray chamber in a conventional slab phantom using the 70 kV spectrum. The depth varied between 0 mm to 30 mm in 10 mm steps. For each point i, the averaged data $\dot{D}_{i,1}$ and $\dot{D}_{i,2}$ were compared for $I_1 = 3$ mA and $I_2 = 10$ mA. The uncertainty was calculated using the average relative deviations.

$$\sigma_\mathrm{c} = \frac{1}{n} \cdot \sum_i^n \frac{\dot{D}_{i,1} - \dot{D}_{i,2} \cdot \frac{I_1}{I_2}}{\dot{D}_{2,i}} \tag{1}$$

Filling pieces for the scintillation detector One mount with five holes was used to estimate the uncertainty caused by the small differences in the shapes of the filling pieces. The scintillation detector was placed into the second hole and irradiated with x-rays through the back of the phantom. The fluctuation of the measured current was analyzed for all filling pieces and their possible orientations by placing the filling pieces between the detector and the entry surface of the x-rays. The relative uncertainty was considered as $\sigma_\mathrm{fs} = \frac{\sigma_I}{\mu_I}$ and measured for the 70 kV spectrum.

Filling pieces for the soft x-ray chamber The amount and combination of filling pieces surrounding the x-ray chamber may cause fluctuation in measured signals. This was analyzed with 20 mm of material in front and 6.5 mm behind the chamber while irradiating into the back of the phantom. Eight different combinations of filling pieces with a varying number of 1 to 12 pieces were employed between the entry surface and detector. The dose rate was measured three times each and averaged. The relative uncertainty was

considered as $\sigma_{fc} = \frac{\sigma_{\dot{D}}}{\mu_{\dot{D}}}$. The measurement was performed with the 100 kV spectrum.

X-ray tube The x-ray tube had to be replaced during the period the measurements were taken. To correct and compare results, a depth dose curve in a conventional slab phantom was taken with both x-ray tubes within the same therapy unit. Dose rates measured with the soft x-ray chamber were recorded for both spectra. The depth varied between 0 mm to 30 mm in 10 mm steps. For each spectrum, the average ratio of dose rates was calculated using

$$r^U = \frac{1}{n} \cdot \sum_i^n \frac{\dot{D}_{i,1}}{\dot{D}_{i,2}} \tag{2}$$

with i describing the depth. All data taken with the second superficial x-ray therapy unit were normalized with r^U.

2.4.2. Measurements to analyze dose profiles

To analyze the impact of a silver plaque on the dose profile, measurements were performed with both spectra. Either the CCB dummy applicator or a PWLR duplicate with the same dimensions was inserted into the phantom, and irradiation was performed from the front or back of the phantom. With three detector types, this leads to a total of 24 data sets.

2.4.3. Calculation of combined depth dose curves

To illustrate the dosimetric benefit, depth dose curves for the combination of brachytherapy and x-ray therapy were calculated for several tumor heights. For brachytherapy, the data were obtained from BEBIG (2013), in which a normalized dose curve D_{norm} was provided by the manufacturer. For x-rays, the data of the presented 100 kV film measurements were taken. The following assumptions were made for this example. The eye was regarded as a sphere with a diameter of 24 mm. Both the tumor and the ^{106}Ru plaque were assumed to be exactly opposite the entry surface of the x-rays. The sclera thickness was defined as $h_{sclera} = 1$ mm. The x-axis was scaled for the x-rays so that a depth of 0 mm corresponds to the radiation entering the eye and 24 mm to the impact on the ruthenium applicator. With a given tumor height of h_{tumor}, this means the tumor apex could be computed to be located in a depth d of $d_{apex} = 24\text{ mm} - h_{sclera} - h_{tumor}$. To combine both data sets, they were fitted using

$$D_{norm}(d) = \exp(a_1 \cdot d^2 + a_2 \cdot d + a_3) \quad \text{for brachytherapy, and} \tag{3}$$

$$\dot{D}(d) = a_1 \cdot d^3 + a_2 \cdot d^2 + a_3 \cdot d + a_4 \quad \text{for x - rays.} \tag{4}$$

Each data set was further normalized to 100 Gy at the tumor apex and then multiplied with a weight w_{x-ray} or $w_{brachy} = 1 - w_{x-ray}$. The combined depth dose curve was then calculated by the sum of the two data sets:

Table 1. Uncertainties measured with the PWLR phantom or provided by the manufacturer, as well as the average ratio of dose rates r^U for both spectra. In addition, the uncertainty of the calibration factor for the soft x-ray chamber $\sigma_{calibration}$, the general uncertainty of values measured with the chamber $\sigma_{chamber}$, the general uncertainty of dose values calculated with the help of radiochromic film σ_{film}, and the general uncertainty of currents acquired with the scintillation detector σ_{szint} are listed.

Uncertainty	Value
$r^{70\text{ kV}}$	0.983(0.003)
$r^{100\text{ kV}}$	0.989(0.003)
σ_c	0.50%
σ_p	0.48%
σ_{fc}	0.15%
σ_{fs}	0.31%
$\sigma_{calibration}$ PTW (2022b)	2.00%
$\sigma_{chamber}$ PTW—PTW Freiburg GmbH (2016)	0.50%
σ_{film} Ashland—Ashland Inc. (2023b)	2.00%
σ_{szint} Eichmann (2010)	1.60%

$$D_c = \frac{D_{norm}(d)}{D_{norm}(h_{apex})} \cdot 100\text{ Gy} \cdot w_{brachy} + \frac{\dot{D}(d)}{\dot{D}(h_{apex})} \cdot 100\text{ Gy} \cdot w_{x-ray}. \tag{5}$$

3. Results

3.1. Uncertainties

The uncertainties based on our phantom, repositioning, or the x-ray tube replacement were in the range of 0.03% to 0.5%, as shown in table 1. Therefore, the systematic uncertainties of the detectors of around 2% dominated the overall uncertainties.

3.2. Dose profiles and the effect of the silver plaque

The depth dose curves measured with all three detector systems are presented in figures 4 and 5. All depth dose curves with an inserted PWLR plaque show the expected exponential decrease over distance, including the data taken with the scintillation detector. The film measurement results reveal larger and more frequent fluctuations than the other two detector types. The biggest differences are observed for absolute dose rates measured with the films for 100 kV irradiation. Compared to the soft x-ray chamber, the dose rate measured with the radiochromic film is up to 35% lower (see figure 5). Measurements with the 70 kV spectrum show less deviations (see figure 4). The dose rates acquired with the radiochromic film are up to 20% lower than those obtained with the soft x-ray chamber. Those deviations were highest in the distances from 0 mm to 20 mm.

Implementing the silver dummy into the phantom significantly decreases the signal at detector positions behind the plaque. Furthermore, in the range of 0 mm to 4 mm directly before the plaque, the dose rate is increased for both spectra. The same effects are better exemplified in figure 6, in which the dose rate ratios

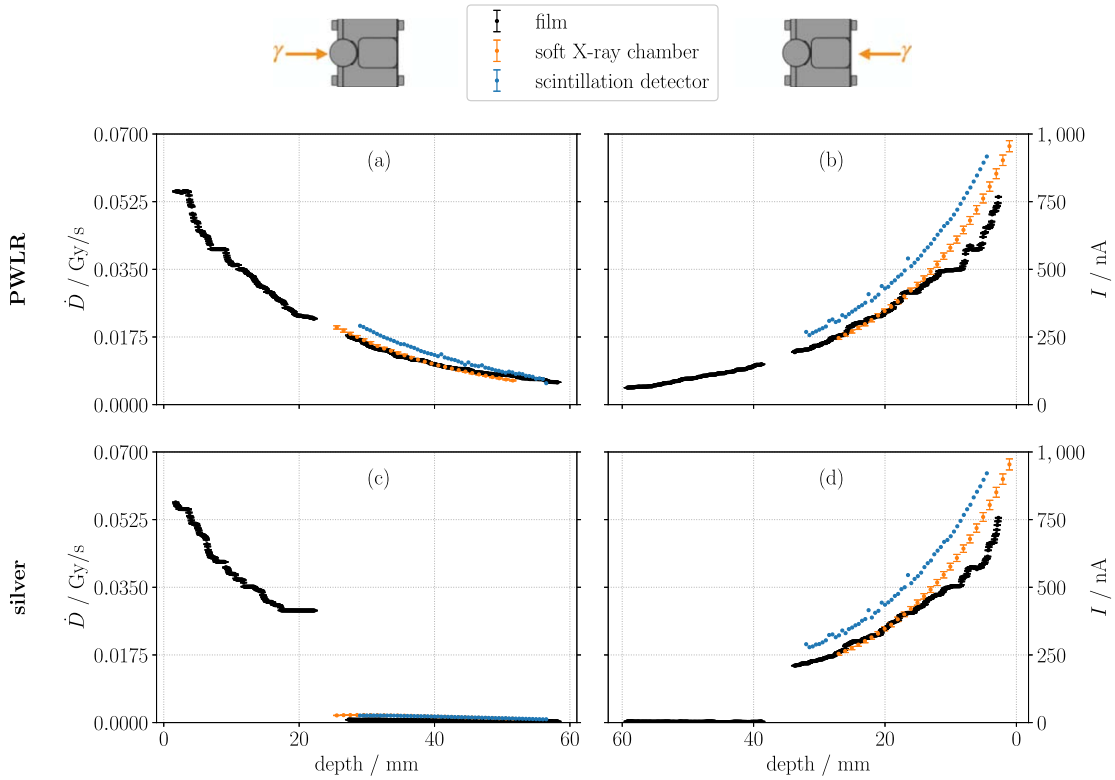

Figure 4. Depth dose curves for the 70 kV spectrum obtained with three different detector types. Values of the soft x-ray chamber and the films are associated with the left y-axes, while values of the scintillation detector are associated with the right y-axes. (a) and (c) show the results for front irradiation, (b) and (d) for back irradiation. In (a) and (b) the PWLR plaque is used, while (c) and (d) were performed with the ^{106}Ru dummy inserted.

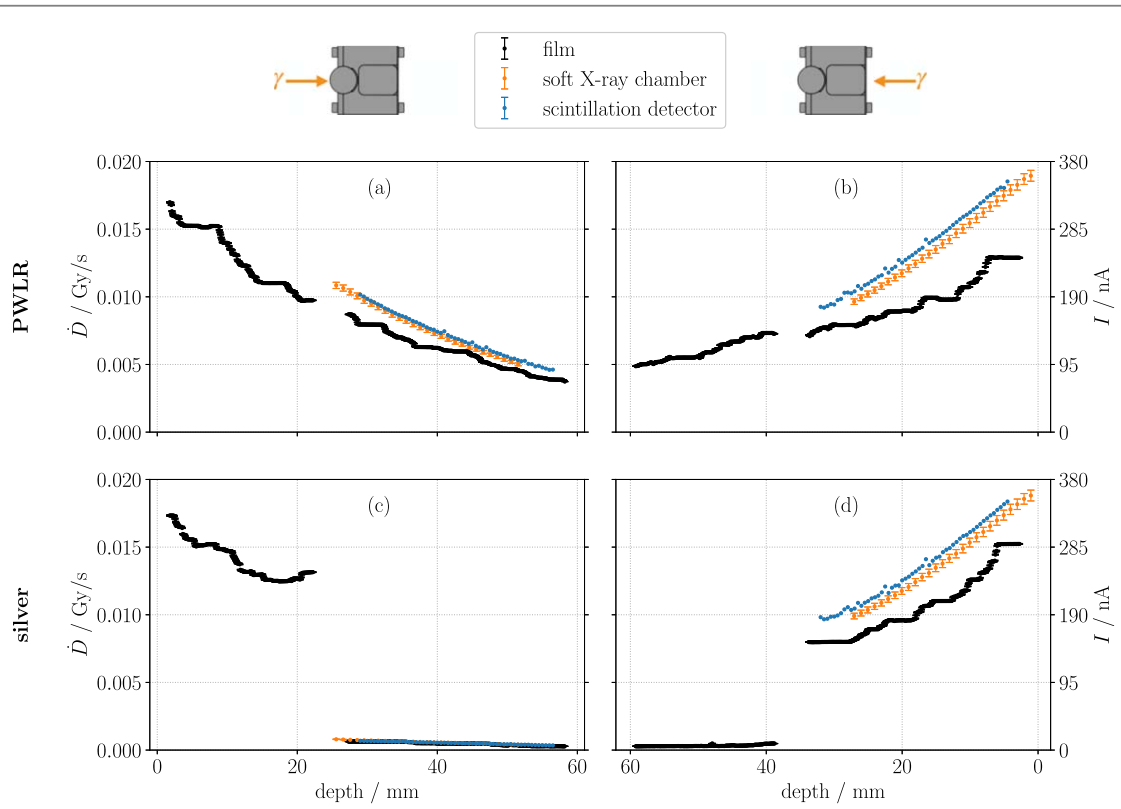

Figure 5. Depth dose curves for the 100 kV spectrum obtained with three different detector types. Values of the soft x-ray chamber and the films are associated with the left y-axes, while values of the scintillation detector are associated with the right y-axes. (a) and (c) show the results for front irradiation, (b) and (d) for back irradiation. In (a) and (b), the PWLR plaque is used, while (c) and (d) were performed with the ^{106}Ru dummy inserted.

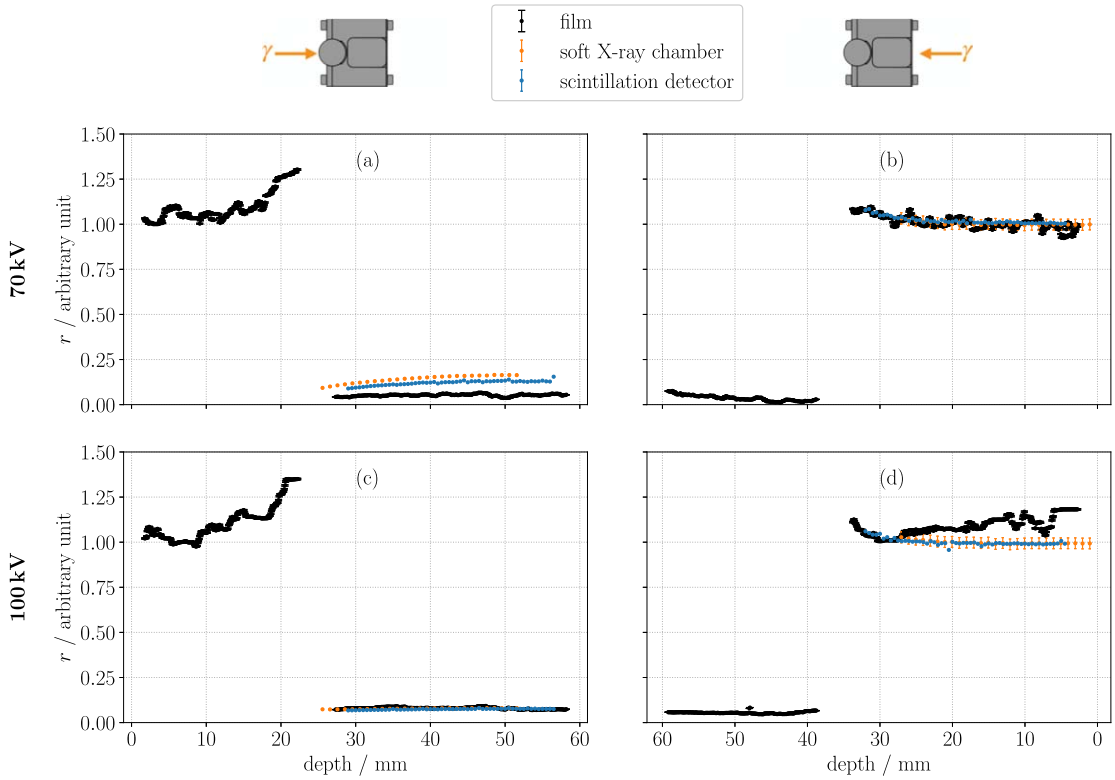

Figure 6. Ratios of the dose rates $\frac{\dot{D}_{\text{silver}}}{\dot{D}_{\text{PWLR}}}$ and currents $\frac{I_{\text{silver}}}{I_{\text{PWLR}}}$. The results from measurements with the 70 kV spectrum are displayed in (a) and (b), and for the 100 kV spectrum in (c) and (d). In a) and (c), the results with front irradiation are shown, while in (b) and (d), results with back irradiation are presented.

$\frac{\dot{D}_{\text{silver}}}{\dot{D}_{\text{PWLR}}}$ and current ratios $\frac{I_{\text{silver}}}{I_{\text{PWLR}}}$ are shown for each detector type, respectively. Both ratios show a relative dose or current increase of up to approximately 35% just before the plaque. Due to the spherical shape of the plaque, this effect is more substantial for front irradiation. In addition, the ratios reveal a significantly decreased dose behind the plaque due to the absorption by the silver plaque. For the 100 kV spectrum, $<$10% of the dose rate reaches the area behind the silver plaque in comparison to no beam stop in the way of the particles. Concerning the 70 kV spectrum, up to 18% of the primary dose is deposited.

3.3. Combined depth dose curves

In figure 7, the calculated depth dose curves for the combination of brachytherapy and x-ray therapy are shown. The dose homogeneity in the tumor volume increases due to the additional x-rays. Especially for larger tumor heights, brachytherapy results in very high dose values of several thousand Gy close to the ^{106}Ru plaque. This underlines previous results that tumors larger than 7 mm can not be treated with brachytherapy due to the dose inhomogeneity. However, with the dose boost applied with x-rays and the corresponding more homogeneous dose profile, larger tumors can be treated without reaching such dose values in certain eye parts. The additional x-ray therapy also leads to increased dose values in the healthy tissue of the eye, which is located before the tumor. In this simple example, only a single field of x-rays is used to irradiate the tumor apex, which results in an exposure of healthy tissue with approximately 100 Gy or more.

4. Discussion

A new combined therapy concept for ophthalmic tumors, which consists of both brachytherapy with ^{106}Ru plaques low-energy x-rays, was presented. In this concept, the plaque irradiates the tumor base while confocal x-rays focus on the remainder of the tumor, e.g. the tumor apex. With the x-rays chosen accordingly, they hit the plaque after passing the tumor volume. As the plaque consists of silver, it resembles a beam stop.

With this concept, the radiotherapeutic options could be extended and highly prominent tumors could be irradiated with another approach than charged particle irradiation or stereotactic radiosurgery. We estimate that the acquisition costs are lower than for proton therapy or the stereotactic approach. This means the combined therapy concept is feasible for more clinics.

Furthermore, the new approach of combining brachytherapy and x-rays might improve the side effect rates and the tumor control rate of ophthalmic

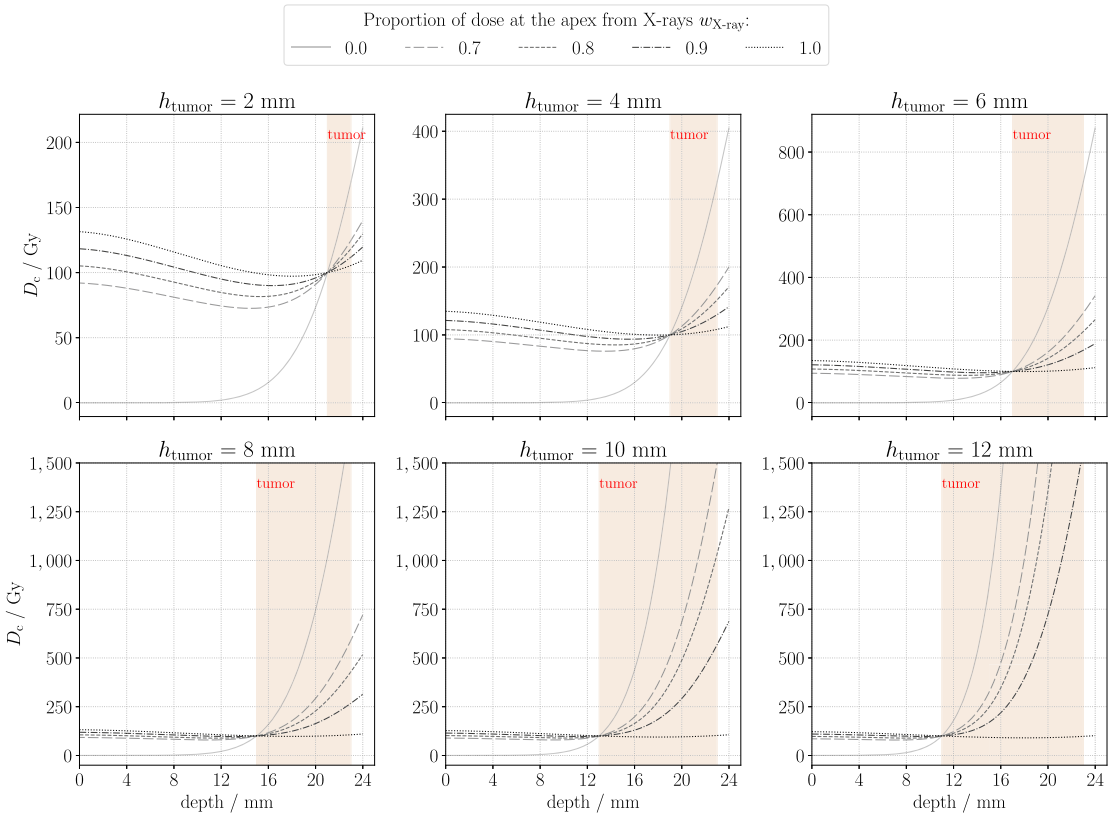

Figure 7. Calculated depth dose curves for the combined therapy concept as a function of tumor height and the proportion of dose at the tumor apex provided by the x-rays $w_{\text{x-ray}}$. The combined depth dose curves are computed as a weighted sum of published data of a ^{106}Ru plaque of type CCB and measured data of a single field of x-rays. The dose curves are normalized to 100 Gy at the tumor apex. The red area resembles the tumor. Due to illustration reasons, an upper y-axis limit of 1500 Gy is used for tumor heights of $h_{\text{tumor}} \geqslant 8$ mm.

tumor treatment. Of course, this has to be proven with a prospective clinical study.

The estimated duration of treatment involving x-rays is challenging to determine precisely, given its considerable dependence on various variables such as focal skin distance, collimator length, field size, and prescribed dose. Preliminary calculations suggest a total treatment time ranging in the order of tens of minutes, comfortably falling below the one-hour threshold. Ongoing and future endeavors are oriented toward optimizing treatment procedures to minimize the overall duration.

A phantom was constructed to investigate the suitability of a ^{106}Ru applicator as a beam stop using three different detector types. Measurements were performed on a T-105 x-ray therapy unit with EBT3 film, a soft x-ray ionization chamber, and a self-made scintillation detector. The results confirm the functionality of the plaque to absorb x-rays and spare healthy tissue behind it. The relative dose increase shortly before the applicator most likely arises due to backscattering and secondary particles from the interactions with the silver plaque, e.g. Auger electrons and photons from x-ray fluorescence. In forthcoming investigations, Monte Carlo simulations will be conducted to evaluate this dose increase more thoroughly, including the proportional contribution of dose attributable to Auger electrons due to their higher relative biological effectiveness. Nevertheless, Auger electrons exhibit a relatively limited range, predominantly affecting tissues nearby, such as the sclera. It is probable that their impact will be inconsequential, with negligible repercussions on dose escalation. The dose increase is a slight disadvantage, as the x-rays are meant to carry out dose deposition mainly at the tumor apex and need to be considered in treatment planning. However, with confocal irradiation, the increased dose values are expected to be in different positions within the tumor. In addition, the positive dose gradient seen in those depth dose curves in front of the applicator is lower than the dose gradient of an active ^{106}Ru applicator. Consequently, the dose is more homogeneous within the tumor for the combined therapy concept than for the standalone brachytherapy.

Each detector used has its pros and cons. The radiochromic film is very suitable within the phantom, as it can be shaped in any form. Therefore, the film can be positioned in many different ways if the corresponding brackets are constructed. In particular, the film is the only detector type that fits in front of the concave side of the applicator. However, the film showed deviations from values obtained with the soft x-ray chamber. Among other things, this could be due to an

energy dependency that was not considered in this analysis (Hammer *et al* 2017). Furthermore, the geometry of the film might have an influence on the measured values if the film is placed parallel to the beam. This has to be both investigated and considered in future measurements. A future version of the phantom shall have a small angle between the radiochromic film and the *z*-axis of the phantom to reduce the effect of the film on the measured depth dose curve, as stated by Vatnitsky (1997), Butson *et al* (2000), Piermattei *et al* (2000), Morris *et al* (2006), Zhao and Das (2010). Due to the absorption of the x-rays in the plaque, some of the applied dose values are lower than the minimum range specified by the manufacturer. To increase radiation time in order to gain as much dose as needed was not feasible. Despite all efforts, it could not be guaranteed that the scan direction of the films was always maintained. In the future, the films will receive a second cutout so that the scan direction can be verified via the position of the two cutouts in relation to each other. Considering all aspects, the uncertainty on dose values obtained with radiochromic film is underestimated. A more comprehensive calculation, as published in, e.g., Bouchard *et al* (2009), shall be included in the future.

The values acquired with the soft x-ray chamber appear to be the most reliable. However, the geometry of the chamber does not allow it to be placed within the curvature of the ^{106}Ru applicator to verify the dose increase. The scintillation detector has the same disadvantage. In addition, it is not calibrated. This means the measurement of an absolute dose rate is not yet possible. For future measurements, a calibration as performed in Ebenau (2017) for a similar scintillation detector can be performed to reevaluate the scintillation detector system regarding dose rate calculations for x-rays.

The presented depth dose curves of the combined therapy concept show the dosimetric benefit the combination of brachytherapy and x-ray therapy provides for tumors with heights >7 mm. By carefully choosing the proportions of the dose applied by the two modalities, large tumors can be treated without exceeding the maximum tolerable sclera dose of usually 1000 Gy to 1500 Gy. The provided example also reveals the exposure of healthy tissue in the eye before the tumor, as dose values of approximately 100 Gy can be observed. However, this example was calculated using a single field. With confocal irradiation, this value can be considerably decreased.

The following aspects must be analyzed before the therapy can be applied in clinical usage. First, the x-ray unit must be mounted to a robot arm with low position uncertainty. To spare the healthy tissue near the pars plana and the planning target volume, the cross-section of the x-ray beams should not exceed a diameter 5 mm. In addition, an investigation regarding field size, collimator length, and similar parameters will be performed to optimize the beam shape for the combined therapy concept. This analysis will also include lateral dose profiles in different depths to evaluate proper tumor coverage. Eye movement is known to be a significant uncertainty for teletherapy. To guarantee correct irradiation, there are two possibilities to overcome the uncertainty of eye movement during the x-ray therapy. One is eye observation with a camera system, and the other is fixation of the eye. As the patient is given a local anesthetic during brachytherapy, we assume the fixation of the eye is the best opportunity and might be adapted from the ORAYA system, presented by Lee *et al* (2008). Meanwhile, camera systems are already used in particle therapy for ophthalmic tumors and represent an alternative to the fixation system (Hrbacek *et al* 2016, Mishra *et al* 2020). Until now, no treatment planning system exists that can combine dose calculations for brachytherapy and an x-ray unit. Therefore, after evaluating the benefits of this concept, such software must be developed to allow for precise planning.

Highly prominent tumors sometimes show irregular shapes. Therefore, the incident x-rays must be carefully planned to cover as much tumor volume as possible and still hit the applicator. Individual consideration of all available modalities is essential for the best outcome.

Results regarding the dose rate effects in ocular brachytherapy show no statistically significant effect (Mossböck *et al* 2007, Fili *et al* 2014, Naseripour *et al* 2016). The biological effectiveness of the x-rays is correlated to the number and frequency of fractions (Fowler 1989, Joiner and van der Kogel 2018). Therefore, this has to be considered to decide how many fractions are to be used within the timing window the brachytherapy provides. The combination of medium dose rate or high dose rate brachytherapy with teletherapy is already used for other tumor entities but new for ophthalmic tumors (Han *et al* 1996, Kouvaris *et al* 1996, Mock *et al* 2003, Samea and Lourenço 2011, Rijkmans *et al* 2017). Also, reports on high single-dose therapies exist (Chan *et al* 2007, Fritz *et al* 2008, Moulding *et al* 2010). A mathematical model to describe the effect of the combination of teletherapy and brachytherapy is already available and can be used in future therapy planning systems (Jones and Bleasdale 1994). Hence, the decision on the number of fractions must consider the radiobiological effectiveness of both modalities. The maximum number of fractions is given due to the application time of the brachytherapy and the clinically feasible number of fractions per day.

A tool to analyze the dosimetric benefit has to be developed. Our current projects include creating Geant4 simulations with retrospective patient data to compare brachytherapy and the combined therapy concept on the basis of depth dose curves and dose volume histograms. The first results are published in Ref. Manke (2023).

5. Conclusion

A novel therapy concept for ophthalmic tumors was presented. It combines ^{106}Ru brachytherapy and low-energy x-rays. The latter is performed in the timing window between application and extraction of the ^{106}Ru applicator. The applicator as a 1 mm thick silver plaque can serve as a beam stop for the x-rays. This was proven with measured depth dose curves in a phantom made of PWLR, which can be used with three different detector types: a soft x-ray ionization chamber, radiochromic film, and a self-made scintillation detector. A first calculation of depth dose curves for a combination of brachytherapy and x-rays showed the dosimetric advantages of the combined concept compared to standalone brachytherapy. We will further investigate the dosimetric benefit of the combined therapy concept for intraocular tumors.

Acknowledgments

We thank WOLF-Medizintechnik GmbH, particularly Christoph Kaufmann, for their collaboration and the gracious opportunity to conduct measurements at their facility using their equipment. Additionally, we extend our gratitude to Carmen Schulz of Eckert & Ziegler BEBIG GmbH for providing the dummy applicator. Special thanks are also extended to Matthias Domke, Jens Sparfeld, and Dirk Schemionek for their valuable assistance in producing and cutting detector components. Acknowledgment is also due to the students who contributed to various aspects of this project, including the construction of scintillation detectors. We are grateful for the support from the TU Dortmund construction office and mechanical workshop in the design and construction of the phantom. We commemorate Bernhard Spaan, who significantly influenced this project with his ideas and knowledge.

Data availability statement

All data that support the findings of this study are included within the article (and any supplementary files).

Funding

The German Research Foundation funded this work as part of project number 455163177.

Conflict of interest disclosure

The authors have no conflict of interest to report.

ORCID iDs

H Manke https://orcid.org/0000-0003-2542-438X
M Stroth https://orcid.org/0009-0000-7241-5887

References

Ashland—Ashland Inc. 2023a Dosimetry Media, Type EBT-3. Tech. rep. Former Gafchromic Inc. (http://gafchromic.com/gafchromic-film/radiotherapy-films/EBT/index.asp)

Ashland—Ashland Inc. 2023b Efficient Protocols for Accurate Radiochromic Film Calibration and Dosimetry. Product specification. Tech. rep. Former Gafchromic Inc.

Bé M-M *et al* 2016 Table of radionuclides *Monographie BIPM-5. Pavillon de Breteuil, F-92310 Sévres* vol 8 (Bureau International des Poids et Mesures)

BEBIG Medical—BEBIG Medical GmbH 2023 T-105—Efficient Application for Superficial X-Ray Therapy (https://bebigmedical.com/products_27/89.html)

BEBIG 2013 Ru-106 Augenapplikatoren Gebrauchsanweisung. Rev. 11-09.2013

Böker A *et al* 2018 Neoadjuvant proton beam irradiation vs. adjuvant ruthenium brachytherapy in transscleral resection of uveal melanoma *Graefe's Archive for Clinical and Experimental Ophthalmology* **256** 1767–75

Bornfeld N *et al* 2004 Perspektiven der ophthalmoonkologie *Deutsches Ärzteblatt* **101** 2526–35

Bouchard H *et al* 2009 On the characterization and uncertainty analysis of radiochromic film dosimetry *Med. Phys.* **36** 1931–46

Butson M J, Cheung T and Yu P K N 2000 Radiochromic film dosimetry in water phantoms *Phys. Med. Biol.* **46** N27–31

Chan S, Dhadda A S and Swindell R 2007 Single fraction radiotherapy for small superficial carcinoma of the skin *Clinical Oncology* **19** 256–9

CIRS—Computerized Imaging Reference Systems Inc 2023 Plastic Water®. Tech. rep. PW DS 120418 (http://cirsinc.com/wp-content/uploads/2019/04/PW-DS-120418.pdf)

Damato B 2023 Therapeutic modalities for uveal melanoma and retinoblastoma: pros and cons *White Paper* ed Eckert & Ziegler BEBIG GmbH

Damato B, Kacperek A, Errington D and Heimann H 2013 Proton beam radiotherapy of uveal melanoma *Saudi Journal of Ophthalmology* **27** 151–7

Desjardins L *et al* 2011 Treatment of uveal melanoma by accelerated proton beam *Current Concepts in Uveal Melanoma. S. Karger AG* **49** 41–57

Ebenau M 2017 Entwicklung eines Binuklidapplikators für die Brachytherapie von Augentumoren und Untersuchungen zur Dosimetrie von Augenapplikatoren *PhD Thesis* TU Dortmund University

Eckert & Ziegler BEBIG GmbH 2022 Ru-106 Eye Applicators. Beta Radiation for Eye Tumor Treatment P13D118/Rev.08 (https://medical.ezag.com/wpcontent/uploads/2021/07/Fact-sheet-Ru-106-Eye-Applicators-Rev.08-English_WEB.pdf)

Eibl-Lindner K *et al* 2016 Robotic radiosurgery for the treatment of medium and large uveal melanoma *Melanoma Research* **26** 51–7

Eichmann M 2017 Inhomogeneous surface dose distributions of 106-Ru eye plaques *Ocular Oncology and Pathology* **4** 21–2

Eichmann M 2010 Entwicklung eines hochpräzisen Dosimetriesystems zur Messung der Oberflächendosisverteilung von Augenapplikatoren *PhD Thesis* TU Dortmund University

Fili M *et al* 2014 High dose rate and low dose rate ruthenium brachytherapy for uveal melanoma *No association with ocular outcome. In: British Journal of Ophthalmology* **98** 1349–54

Fleury E *et al* 2021 Characterization of the HollandPTC proton therapy beamline dedicated to uveal melanoma treatment and an interinstitutional comparison *Med. Phys.* **48** 4506–22

Flühs D *et al* 2004 The design and the dosimetry of bi-nuclide radioactive ophthalmic applicators *Med. Phys.* **31** 1481–8

Foti P V *et al* 2021 Diagnostic methods and therapeutic options of uveal melanoma with emphasis on MR imagingPart II: treatment indications and complications *Insights into Imaging* **12** 67
Fowler J F 1989 The linear-quadratic formula and progress in fractionated radiotherapy *The British Journal of Radiology* **62** 679–94
Fritz P *et al* 2008 Stereotactic, high single-dose irradiation of stage I nonsmall cell lung cancer (NSCLC) using four-dimensional CT scans for treatment planning *Lung Cancer* **60** 193–9
Gravotech GmbH 2022 Lasergravierer & Cutter. LS900. Tech. rep. Gravotech- LS900-11-2022-de-DE
Hamamatsu Photonics K K 2016 *H10720/H10721 Series. Photosensor Modules. Tech. rep. TPMO1062E02*
Hamamatsu Photonics K K 2023 H10721-210. Photomultiplier tube module (https://hamamatsu.com/jp/en/product/optical-sensors/pmt/pmt-module/currentoutput-type/H10721-210.html)
Hammer C G *et al* 2017 Experimental investigation of GafChromic® EBT3 intrinsic energy dependence with kilovoltage x rays, 137Cs, and 60Co *Med. Phys.* **45** 448–59
Han I *et al* 1996 Multifractionated high-dose-rate brachytherapy with concomitant daily teletherapy for cervical cancer *Gynecologic Oncology* **63** 71–7
Hrbacek J *et al* 2016 Practice patterns analysis of ocular proton therapy centers: the international OPTIC survey *International Journal of Radiation Oncology—Biology - Physics* **95** 336–43
Joiner M C and van der Kogel A J (ed) 2018 *Basic Clinical Radiobiology* (CRC Press)
Jones B and Bleasdale C 1994 Effect of overall time when radiotherapy includes teletherapy and brachytherapy: a mathematical model *The British Journal of Radiology* **67** 63–70
Kouvaris J *et al* 1996 Combined teletherapy and intracavitary brachytherapy boost for the treatment of nasopharyngeal carcinoma *Radiother. Oncol.* **38** 263–7
Lee C *et al* 2008 Dosimetry characterization of a multibeam radiotherapy treatment for age-related macular degeneration *Med. Phys.* **35** 5151–60
Lommatzsch P K and Vollmar R 1966 A new way in the conservative therapy of intraocular tumors by means of beta-irradiation (Ruthenium 106) with preservation of vision *Klinische Monatsblätter fur Augenheilkunde* **148** 682–99
Manke H 2023 Brachytherapy meets X-rays. a novel concept to treat ophthalmic tumours *PhD Thesis* TU Dortmund University
Mazzini C *et al* 2020 Clinical outcomes and secondary glaucoma after gamma-knife radiosurgery and Ruthenium-106 brachytherapy for uveal melanoma: a single institution experience *Melanoma Research* **31** 38–48
Mishra K K *et al* 2020 Practice considerations for proton beam radiation therapy of uveal melanoma during the coronavirus disease pandemic: particle therapy co-operative group ocular experience *Advances in Radiation Oncology* **5** 682–6
Mock U *et al* 2003 High-dose-rate (HDR) brachytherapy with or without external beam radiotherapy in the treatment of primary vaginal carcinoma: Longterm results and side effects *International Journal of Radiation Oncology—Biology - Physics* **56** 950–7
Mor J M *et al* 2017 CyberKnife®: eine neue therapieoption bei uvealem melanom *Der Ophthalmologe* **115** 302–8
Morris K N, Weil M D and Malzbender R 2006 Radiochromic film dosimetry of contrast-enhanced radiotherapy (CERT) *Phys. Med. Biol.* **51** 5915–25
Mossböck G *et al* 2007 Impact of dose rate on clinical course in uveal melanoma after brachytherapy with ruthenium-106 *Strahlentherapie und Onkologie* **183** 571–5
Moulding H D *et al* 2010 Local disease control after decompressive surgery and adjuvant high-dose single-fraction radiosurgery for spine metastases *Journal of Neurosurgery: Spine* **13** 87–93
Naseripour M *et al* 2016 Ruthenium-106 brachytherapy for thick uveal melanoma: reappraisal of apex and base dose radiation and dose rate *Journal of Contemporary Brachytherapy* **8** 66–73
Open CV 2022 Open Source Vision Foundation (Dec. 29, 2022). Hough Circle Transform
Open CV 2023 Creating Bounding rotated boxes and ellipses for contours
Paganetti H 2012 *Proton Therapy Physics* (CRC Press)
Piermattei A *et al* 2000 Radiochromic film dosimetry of a low energy proton beam *Med. Phys.* **27** 1655–60
PTW—PTW Freiburg GmbH 2016 Gebrauchsanweisung. Weichstrahlkammern Typ 34013, Typ 23342 und Typ 23344. Tech. rep. D564.151.00/005 de
PTW 2020 UNIDOS®Romeo *User manual* Tech. rep. D970.236.01/00 de
PTW 2021 *UNIDOS® Tango & Romeo. The New Generation of Reference Class Electrometers* Tech. rep. D970.139.00/02 2021-10
PTW 2022b *Kalibrierschein* Tech. rep. 220317701
PTW 2023 UNIDOS® Tango and UNIDOS® Romeo (https://ptwdosimetry.com/en/products/unidos-tango-and-unidos-romeo/)
Rauchegger T *et al* 2020 Zehn Jahre multimodale Therapie uvealer Melanome an der Universitätsaugenklinik Innsbruck *Spektrum der Augenheilkunde* **34** 18–25
Rijkmans E C *et al* 2017 Endorectal brachytherapy boost after external beam radiation therapy in elderly or medically inoperable patients with rectal cancer: primary outcomes of the phase 1 HERBERT study *International Journal of Radiation Oncology—Biology - Physics* **98** 908–17
Samea R and Lourenço L G 2011 Comparação dos tratamentos do carcinoma espinocelular avançado do esofago pela teleterapia exclusiva e pela teleterapia associada à braquiterapia *ABCD. Arquivos Brasileiros de Cirurgia Digestiva (São Paulo)* **24** 267–71
Schmelter V *et al* 2022a Robotic CyberKnife radiosurgery for small choroidal melanomas *Melanoma Research* **32** 192–9
Schmelter V *et al* 2022b Local recurrence in choroidal melanomas following robotic-assisted radiosurgery (CyberKnife) *Ocular Oncology and Pathology* **8** 221–9
Seibel I *et al* 2015 Local recurrence after primary proton beam therapy in uveal melanoma: risk factors, retreatment approaches, and outcome *American Journal of Ophthalmology* **160** 628–36
Sekac J *et al* 2019 Secondary glaucoma in small versus large uveal melanoma patients treated with stereotactic radiosurgery on linear accelerator *Bratislava Medical Journal* **120** 945–9
Sommer H *et al* 2017 Monte Carlo simulation of ruthenium eye plaques with GEANT4: influence of multiple scattering algorithms, the spectrum and the geometry on depth dose profiles *Phys. Med. Biol.* **62** 1848–64
Stöckel E *et al* 2017 Dose distributions and treatment margins in ocular brachytherapy with 106Ru eye plaques *Ocular Onthology and Pathology* **4** 122–8
Tagliaferri L *et al* 2020 Uveal melanoma *The GEC ESTRO Handbook of Brachytherapy* ed E van Limbergen (ESTRO)
Tarlan B and Kıratlı H 2016 Uveal melanoma: current trends in diagnosis and management *Turkish Journal for Ophtalmology* **46** 123–37
The Collaborative Ocular Melanoma Study Group 2001 The COMS randomized trial of iodine 125 brachytherapy for choroidal melanoma, III: initial mortality findings. COMS Report No. 18 *Arch Ophthalmol.* **119** 969–82
Tseng V *et al* 2016 Complications from plaque versus proton beam therapy for choroidal melanoma: a qualitative systematic review *Journal of Cancer Therapy* **7** 169–85
Vatnitsky S M 1997 Radiochromic film dosimetry for clinical proton beams *Appl. Radiat. Isot.* **48** 643–51
WOMed—Wolf-Medizintechnik GmbH 2023 T-105: Equipment for superficial x-ray therapy. Efficient applicaton for superficial x-ray therapy (https://bebigmedical.com/static/upload/file/20221027/1666852967785658.pdf)
Zhao L and Das I J 2010 Gafchromic EBT film dosimetry in proton beams *Phys. Med. Biol.* **55** 291–301